COVER SHEET

Investigation on the delaminated-pillared structure of TiO_2-PILC synthesized by $TiCl_4$ hydrolysis method

Peng YUAN,[1] Xiaoling YIN,[1,2] Hongping HE,[1*] Dan YANG,[1,2] Linjiang WANG [3] Jianxi ZHU [1]

1 Guangzhou Institute of Geochemistry, Chinese Academy of Sciences, Guangzhou 510640, China

2 Graduate School of the Chinese Academy of Sciences, Beijing 100039, China

3 Key Laboratory of Nonferrous Materials and Processing Technology (Guilin University of Technology), Ministry of Education, Guilin 541004, China

TiO_2-PILCs were synthesized by the reaction between montmorillonite and acidic solutions of hydrolyzed $TiCl_4$. Unlike commonly reported microporous pillared structure, a meso-microporous delaminated structure containing pillared fragments was observed in the resulting TiO_2-PILC, based on the combined analyses of powder X-ray diffraction (XRD), nitrogen adsorption-desorption isotherms, chemical analysis, thermogravimetric (TG) and differential scanning calorimetry (DSC) analyses. Air-drying after ethanol extraction (EAD) is shown to be more effective than air-drying (AD) in preserving the delaminated structure in the resultant Ti-clay. A broad XRD peak at low 2θ angle with a high *d*-spacing of ca. 6.6 nm was firstly reported and it was proposed to be correlated with the mesoporous delaminated structure rather than the (001) reflection of intercalated/pillared periodic structure. The resulting TiO_2-PILC exhibits a good thermal stability as indicated by its surface area after calcination at 600 °C. Moreover, calcination above 300 °C results in the formation of nanocrystalline anatase in the TiO_2-PILC, and the grain size of anatase increases with the increment of calcination temperature. However, no phase transformation from anatase to rutile was observed even under calcination at 1000 °C. These fundamental results provide new insights about the structure of TiO_2-PILC synthesized by $TiCl_4$ hydrolysis method.

Keywords: TiO_2-PILC; Delaminated structure; Mesoporous-microporous materials; Anatase; Rutile

[*] Corresponding author. *E-mail address*: hehp@gig.ac.cn (H. P. He) Tel: +86 20 85290257; Fax: +86 20 85290130.

1. Introduction

Pillared interlayered clay (PILC) with inorganic particles has attracted great research interest since it was first introduced in the late 1970s [1,2]. Classified as a two-dimensional layer nanomaterial, PILC is prepared by exchanging the charge-compensating cations between the swelling clay layers with larger polymeric or oligomeric hydroxy metal cations. Upon heating, the metal hydroxy cations undergo dehydration and dehydroxylation, forming stable metal oxide (e.g. Al_2O_3, TiO_2, and Fe_2O_3 etc.) clusters. The resultant oxide-PILC shows promising prospects in the fields of adsorbents and catalysts [3-6].

Compared with other types of PILCs, TiO_2-PILC exhibits some attractive advantages in the field of wastewater treatment. For example, TiO_2-PILC can be used as a photocatalyst to degrade or mineralize some persistent organic pollutants to carbon dioxides, water, and mineral ions [7-10], due to its photochemical and photocatalytic properties resulting from the microcrystalline TiO_2 formed under calcination condition [11]. Recently, synthesis and application of mixed oxides containing TiO_2 also attract great interest [12], in which the phase transformation of TiO_2 under calcination [13], and surface TiO_2 structure and its contribution to the surface acidity of the resultant materials were investigated [12].

For a photocatalytic reaction using TiO_2 as photocatalyst, anatase-type TiO_2, rather than the rutile-type TiO_2, was proven to be the active component [14]. The formation of anatase in TiO_2-PILC upon calcination has been noted in some literatures [15.16], whereas it was not found in some other repots [11,17,18]. In addition, Ding et al. reported a supercritical dried TiO_2-PILC containing both anatase and rutile upon calcination at 500 °C [7]. These diverse results indicate that further studies are necessary to have a better knowledge on the formation of anatase in TiO_2-PILC.

Generally two different routes to create Ti complexes suitable for pillaring processes

were reported in the literature [4]. The first one is adding $TiCl_4$ to 5 or 6 M HCl followed by dilution with distilled water and aging from 3 hours up to as long as 20 days prior to being used in pillaring process [15,18,19]. The second is based on the hydrolysis of various Ti alkoxides under relatively mild acidic conditions (mostly 1M HCl) [4,17,20,21]. The interlamellar distance of TiO_2-PILCs synthesized by both hydrolysis methods are commonly reported in the range of 1.4 – 1.9 nm (corresponding to the basal $d_{(001)}$ spacing values of ca. 2.3 – 2.8 nm) [4,22]. These values of interlamellar distance indicate that TiO_2 pillars create a microporous (pore diameter < 2 nm) structure within the interlayer region of TiO_2-PILC. This microporosity of TiO_2-PILC has been widely reported in literature [23].

In this work, TiO_2-PILC was synthesized through the traditional $TiCl_4$ hydrolysis method. And a combined study using powder X-ray diffraction (XRD), nitrogen adsorption-desorption isotherms, thermogravimetric (TG) and differential scanning calorimetry (DSC) analyses was conducted to characterize the resultant TiO_2-PILCs. The influence of two different drying methods on the structure of TiO_2-PILCs was discussed. And the effects of calcination on the structure of TiO_2-PILCs and on the formation of nano-sized anatase were investigated.

2. Experimental

2.1. Materials.

The starting calcium-montmorillonite (Ca^{2+}-Mt) was supplied by Nanhai Mining Ltd., China. It was purified by sedimentation, and the < 2 μm fraction was collected. The chemical formula of the obtained Ca^{2+}-Mt can be expressed as:

$$Ca_{0.19}Mg_{0.06}Na_{0.01}(Si_{3.96}Al_{0.04})\ (Al_{1.44}Fe_{0.09}Mg_{0.47})\ O_{10}(OH)_2{\cdot}nH_2O.$$

Its cationic exchange capacity (CEC) is 66.5 meq/100g. Na^+-exchanged montmorillonite (Na^+-Mt) was prepared by ion exchange reaction between Ca^{2+}-Mt and Na_2CO_3, as previously described [24]. The Na^+-Mt was used as the starting materials for the pillaring reactions.

2.2. Preparation of Ti pillaring solution TiO_2-PILCs.

Following a procedure similar to that reported in the literatures [15,25], the Ti pillaring solution was prepared by adding $TiCl_4$ to a 6.0 M HCl solution, which was diluted in deionized water under vigorously stirring. The concentration of Ti in the obtained solution is 0.82 M, and that of HCl is 1.0 M. The resulting solution was aged for 3 h at room temperature before being added to the Mt suspension. Simultaneously, Na^+-Mt powder was dispersed in 0.5 L of deionized water under stirring for 3 h to obtain a 0.4 % (wt%) suspension.

The Ti pillaring solution was then dropwise added into the vigorously stirred Na^+-Mt suspension until the ratio of Ti/clay up to 20 mmol g^{-1} of clay. After addition of the pillaring solution, the reaction mixture was stirred for an additional 4 h and aged for 12 h at room temperature. The mixture (with a pH value of 0.6) was centrifuged and washed by successive agitations/centrifugations with deionized water, until Cl^- anions free detected by $AgNO_3$ test. The obtained PILC wet cakes were then ready for drying.

2.3. Drying and calcination.

The PILC wet cakes were directly dried (AD) at 105 ^oC for 16 h, or air-dried in the same conditions, but after methanol extraction (EAD). In EAD process, the methanol is used to replace water. The dried samples were calcined for 4 h at different temperatures (300, 400, 500, 600, 700, 800 and 900 °C). The final TiO_2-PILC products were ground into powder with mortar for characterization. They were denoted on the basis of the drying method and the calcination temperature. As a referenced sample, an acid-activated montmorillonite was prepared following a similar synthesis process of TiO_2-PILC, except the $TiCl_4$ was replaced by deionized water. The final acid-activated Mt was calcined at 300 °C for 4 h and hereafter denoted as AA-300.

2.4. Characterization methods

The X-ray diffraction (XRD) patterns were measured with a Rigaku D/max 120

diffractometer using CuKα radiation (λ = 0.154 nm). A Rigaku D/max 2550 PC X-ray diffractometer (CuKα radiation) equipped with a graphite monochromator was used to acquire the low 2θ (0.5 – 10 °) angle XRD patterns of the PILC samples. A fixed power source (40 kV, 300 mA), and a scan rate of 3 degree (2θ)/min were applied for the determination of the low angle XRD. The chemical composition of the samples was determined using a PE-3100 atomic absorption spectrometer (AAS).

Thermogravimetric (TG) and Differential Scanning Calorimetry (DSC) analysis were synchronously performed on a Netzsch STA 449C instrument. Approximately 20 mg of finely ground sample was heated in an open corundum crucible. Samples were heated from 40 to 1300 °C K at a heating rate of 10 °C/min under highly pure nitrogen atmosphere (20 cm^3/min).

N_2 adsorption-desorption isotherms were measured at liquid nitrogen temperature with a gas sorption analyzer (Quantachrome, NOVA 1000). Prior to measurement, samples were outgassed at 250 °C, at a pressure less than 10^{-3} Torr for 3 h. The specific surface area was calculated by the BET equation [26] and the total pore volume was evaluated from nitrogen uptake at a relative pressure of 0.99. The *t*-plot according to De Boer's method was used to calculate the micropore volume and external surface area [27]. The Barrett-Joyner-Halenda (BJH) method was used to evaluate the average pore diameter (APD) [28]. And the pore size distribution (PSD) curves was fitted by the non-local density functional theory (NLDFT) method [29].

3. Results and discussion

3.1. X-ray diffraction and chemical analysis.

Fig. 1 shows the XRD patterns of the Na^+-Mt and the air-dried (AD) TiO_2-PILC samples. In the XRD pattern of Na^+-Mt (Fig. 1a), the intense peak at 2θ = 7.1° (*d* = 1.24 nm) corresponds the (001) reflection, and the peak at 2θ = 21.9 ° (*d* = 0.41 nm) is the

diffraction of (101) from cristobalite impurity. The XRD patterns (Figs. 1c–j) of TiO_2-PILC samples are characterized by the absence of (001) diffraction. A broad peak centered at 25.3 º (d = 0.35 nm) is recorded and its intensity increases with the increment of the calcination temperature. The TiO_2-PILCs (EAD) exhibit analogous XRD patterns (not shown here) to those of air-dried ones

As shown in Fig. 1b, the acid treated sample AA-300 shows a (001) diffraction with basal spacing of ca. 0.97 nm. The existence of this (001) diffraction peak indicates that the periodic interlayer structure is still preserved under the present acidic condition. On the contrary, the XRD patterns of TiO_2-PILCs exhibits almost complete loss of periodic diffraction. This result indicates that the disordered structure of TiO_2-PILCs should not be ascribed to the highly acidic synthesis condition, despite that a small amounts of Al and Si could be removed from the clay structure under acidic condition [15,18].

The diffused XRD pattern observed for TiO_2 PILC indicates a highly disordered structure, similar to that previously observed in Fe_2O_3 pillared clay [30,31] and Al_2O_3-laponite which were referred to as “delaminated clay” [31,32]. In a previous report about TiO_2-PILC, the diffuse XRD pattern was also observed [16]. Nevertheless, the formation mechanism of the diffuse XRD pattern has not been well established.

Bagshaw et al. ascribed the diffuse XRD pattern of TiO_2-PILC to the hydrolysis property of Ti(IV) cations [16], i.e., the presence of a wide range of hydrolyzed species of Ti with different sizes (such as monomeric TiO^{2+}/$Ti(OH)_2^{2+}$ and polymeric species [33,34]) in the pillaring solution causes the nonuniform pillaring of the clay layers [16]. This proposal obtains a strong support from the low 2θ angle XRD patterns of TiO_2-PILC samples as shown in Figs. 1k and l. It can be seen that a broad peak, centered at ca. 1.51 nm for Ti-AD-300 and ca. 1.38 nm for Ti-EAD-300, appears and it should be attributed to the (001) reflection resulting from the periodic stacking of clay layers, indicating the inhomogenous intercalation of the hydrolyzed titanium cations with nonuniform sizes. As a result of this inhomogenous intercalation, different clay particles exhibit different

interlayer distance, leading to broadening of the (001) diffraction.

However, in the same XRD pattern there is also an unexpected broad diffraction peak. A peak corresponding to *d* spacing of 6.64 nm is shown in the XRD pattern of Ti-AD-300, and a similar peak with a *d* spacing of 6.90 nm is recorded in that of Ti-EAD-300 (Figs. 1k and l). A higher distance than those reported in literature, but not so high as reported in this study, is also reported by Bergaya et al. for Ti-PILC [35,36]. This observation is very interesting since such high *d* spacing in the XRD patterns of TiO_2-PILCs synthesized by $TiCl_4$ hydrolysis method has not been reported, to the best of our knowledge.

Mandalia et al observed a *d* spacing of 7.2 nm in the XRD pattern of Fe_2O_3-pillared Mt [37]. However, they proposed that the 7.2 nm peak cannot be attributed to simple intercalation of iron hydroxycations [38], but to the existence of some porous structure. This proposal seems to be reasonable since it may be supported by the fact that some disordered solids show broad XRD peak at very low 2θ angle region, such as porous silica [39], silica molecular sieves [40], and mesoporous biogenetic silica [41]. Analogously, the high *d* spacings shown in the resulting TiO_2-PILCs may be correlated with some disordered porous structure, rather than large interlayer distances of TiO_2-PILCs. The porous structure of the resultant TiO_2-PILCs should be analogous to the so-called "delaminated" structure found in Al_2O_3-PILC [32,42], and result from the three-dimensional coaggregation of clay particles and Ti hydroxycations.

The chemical analysis (Table 1) shows that the TiO_2 content of the resulting TiO_2-PILCs are dramatically higher than that of Na^+-Mt. However, on the assumption that all of the hydrolyzed Ti species (e.g. TiO^{2+}) are intercalated into the interlayer of starting Na^+-Mt, a Ti content only about 2 % will be calculated from the CEC value, much lower than the actually determined Ti content (ca. 16.2 %, deduced from the TiO_2 content 25.57 %). This divergence between the two Ti contents suggests that most of the hydrolyzed species of titanium exist outside rather than inside the clay interlayers. These species may be Ti polyoxycations with large size and they are hard to be intercalated into

the clay interlayer, for instance, they coaggregate with clay particles to form a three-dimensional delaminated structure.

Hence, it could be concluded that two factors are essential in leading to diffuse XRD patterns of the TiO_2-PILCs. One is the nonuniform interlayer distances of clays resulting from inhomogenous intercalation by small-sized Ti hydrolyzed species. The other one is the disordered three-dimensional coaggregation of clay particles and Ti polyoxycations, i.e., the delaminated structure. Accordingly, both delamination and intercalation make contribution to the formation of the disordered structure of TiO_2-PILCs.

The high *d*-spacing exhibited in the low 2θ angle region of XRD patterns shows some correlation with the porosity of the delaminated Ti pillared clay, though its accurate assignment is still difficult. It is noteworthy that a scan beginning at lower 2θ angle may be necessary to investigate the structure of PILCs as underlined by Bergaya et al. [35,36].

3.2. Nitrogen adsorption-desorption isotherms

Figures 2a and b represent N_2 adsorption-desorption isotherms of the Ti-AD-300 and Ti-EAD-300. Both adsorption isotherms belong to Type IV in the Brunauer, Deming, Deming and Teller (BDDT) classification [43], corresponding to a mesoporous structure. In addition, in the region of relatively low pressure both adsorption isotherms exhibit Langmuir adsorption type (type I in BDDT classification), indicating the presence of micropores. Moreover, the hysteresis loops of these two isotherms seem to be of type H3 (IUPAC classification [26]), corresponding to slit-shaped pores in resultant materials. In all smectite clay isotherms, the desorption branch shows an inflection "knee" at about 0.45-0.5 P/Po. This inflection has been observed for many different types of layered materials when using nitrogen as the sorbent gas (nitrogen boils at P/Po 0.42) [5,6,44]. The phenomenon arises due to the complexity of capillary condensation in pore networks with pore blocking effects, and it is sometimes called the tensile strength artifact [45]. Seaton has determined that the spinodal pressures (the point at which liquid in the pore reaches its limit of intrinsic stability and nitrogen vaporizes spontaneously) for a wide

range of pore sizes fall within a narrow range [46]. Therefore, the closure of hysteresis loops occurs at almost exactly the same pressure, which is in fact the tensile strength artifact. According to Sing et al. [45], hysteresis arises in systems containing microporous slit-shaped pores.

As shown in Figures 2c and d**,** the mesopore (pore diameter ≥ 2 nm) size distribution curves of Ti-AD-300 and Ti-EAD-300 show that the size of mesopores in these two samples is not uniform, and most of pore diameter is about 2 – 4 nm. This result is well in accordance with the inhomogeneous pore size of the disordered delaminated structure.

Summarized in Table 2 are the pore structure parameters of the Na^+-Mt and TiO_2-PILC samples, including specific surface area (S_{BET}), external surface area ($S_{ext.}$), total pore volume (V_P), microporous volume ($V_{\mu P}$) and average pore diameter (APD). It can be seen that the pillaring process leads to a dramatic increase in surface area and porosity with respect to that of starting Na^+-Mt, and both mesoporosity and microporosity contribute to the total porosity and surface area in the resultant Ti-PILCs. According to above discussion based on the XRD results, mesopores in Ti-PILCs may result from spaces or pores generated by the 3D co-aggregation of the clay particles and the Ti polyoxycations. In contrast, micropores may have two possible sources: one is from the space between clay particles and the other from the space between the layers, and the other one is from the interlayer pore of Ti-PILC, resulting from the intercalation of small-sized hydrolyzed titanium cations as previously reported [4]. A schematic representation of this delaminated-pillared structure is shown in Fig. 3.

The surface area (250.1 m^2/g) of Ti-AD-300 is consistent with the values reported for Ti_2O_3-PILC [4]. However, unlike the mesoporous-microporous structure exhibited in the present Ti-PILCs, primarily microporous structure was observed in the literature [23]. On the other hand, much more developed surface area and porosity was exhibited in Ti-EAD-300 than Ti-AD-300 (Table 2), indicating EAD method has advantages in producing high surface area over AD method. This result can be explained by the much

lower interfacial tension of ethanol as compared to water, i.e., when water is used for washing, some pores in the delaminated structure might tend to collapse owing to the high interfacial tension of water. However, when water was replaced by ethanol in EAD method, interfacial tension was dramatically reduced so that more porous delaminated structure was preserved. Similar result was observed in the case of Ti-PILC under supercritical fluid drying condition.[5]

3.3. Effects of calcination treatment on the structure of the delaminated Ti pillared clays

As shown in Figs. 4a and b, an increase of calcination temperature from 300 to 700 °C leads to an obvious decrease of the specific surface area of the delaminated Ti pillared Mt. Under calcination at 600 °C, both Ti-AD-600 and Ti-EAD-600 remain high surface area (200.9 and 214.2 m^2/g, respectively), reflecting the delaminated Ti pillared Mt has good thermal stability. However, calcination at 700 °C results in a dramatic decrease in the surface areas of Ti-AD-700 and Ti-EAD-700 (Fig. 4), suggesting the collapse of the porous delaminated/pillared structure.

Another dramatic change occurs in the delaminated Ti pillared Mt under calcination is the formation of anatase phase, as indicated by the XRD patterns (Figs. 1c–j). The XRD patterns show that the intensity of the (101) peak (2θ = 25.3°) of anatase gradually increases with the increase of calcination temperature, reflecting the growth of the crystalline grains of anatase. The mean diameter, D, of the anatase crystallites in calcined Ti-Mt can be roughly estimated by the Scherrer equation: $D=k\lambda/\beta\cos\theta$ [7], where k is the shape factor with the value of 0.9, β is the line broadening which is the width of the diffraction line at its half intensity maximum, λ is the radiation wavelength applied, and θ is the Bragg angle, respectively. As depicted in Fig. 4c, the calculation result shows that the D values of the anatase crystalline grain increase from ca. 10.5 nm (for Ti-AD-300) to 26.6 nm (for Ti-AD-1000), with the increment of calcination temperature. An analogous change is also found in the delaminated Ti pillared Mts under EAD condition (Fig. 4d). Moreover, a noteworthy change shown in the XRD patterns is the obvious increase of the intensity of the cristobalite peak at 1000 °C. This increase should be assigned to the

cristobalite transformed from amorphous silica under calcination at 1000 °C [47], and the amorphous silica might result from the leached Si from the clay structure in the synthesis process [18].

Previous researchers have investigated anatase-to-rutile phase transformation under calcination condition [48,49]. Their results showed that the range of phase transformation temperature are rarely above 1000 °C, commonly in the range of 500 - 900 °C, varying with the preparation route, pressure, particle size, additive, and hydrothermal condition etc. Accordingly, it is unexpected that no phase transformation from anatase to rutile is observed in the delaminated Ti pillared Mt even under calcination temperature at 1000 °C (Fig. 1m). A reasonable explanation to this observation is that clay particles can separate the nanocrystalline anatase particles and thus reduce the effective contact areas between these particles. Many of anatase particles are therefore prevented from aggregating together and further transforming to rutile. Consequently, the delaminated structure shows an interesting function on improving the thermal stability of nanocrystalline anatase.

As shown in Figs. 5a and b, the Ti-AD and Ti-EAD exhibit similar thermogravimetric curves, in which an obvious weight-loss appears at 71 °C, and other two weak ones appears at ca. 550 and ca. 260 °C. The weight-loss at ca 71 °C corresponds to desorption of the physically adsorbed water whereas the other two ones at ca. 260 and 550 °C should be attributed to the dehydroxylation of Ti polyoxycations and the dehydroxylation of structural hydroxyl groups of montmorillonite, respectively.

In the DSC curves (Fig. 5c), three endothermic peaks centered at almost the same positions, similar to the DTG peaks, can be resolved, providing a support to above-mentioned assignment. Moreover, another endothermic peak at ca. 809 °C can be seen at the DSC curve of Ti-EAD, and a similar peak at the DSC curve of Ti-AD is at ca. 720 °C with much weaker intensity. This peak corresponds to the collapse of montmorillonite structure due to the absence of mass loss as indicated by TG curves.

On the other hand, three exothermic peaks centered at ca. 950, 1100, and 1200 °C can be seen at the DSC curves. The one at 950 °C should be attributed to the formation of cristobalite resulting from calcination on montmorillonite. This assignment is supported by the XRD patterns (Figs. 1i and j), which show a dramatic increase in the intensity of cristobalite peak when the calcination temperature increases from 900 to 1000 °C. The peak at 1200 °C corresponds to the formation of mullite phase, also resulting from calcined montmorillonite according to the literature [50]. However, the peak at ca. 1100 °C might correspond to the occurrence of the anatase-to-rutile phase transformation.

Based on above discussion, the resulting TiO_2-PILCs in this work show some properties different from those reported in some previous reports. For instance, we obtained a mesoporous/microporous delaminated-pillared structure by synthesis route of $TiCl_4$ hydrolysis. However, a dominant microporous structure in interlayer region was obtained under similar synthesis method by other researchers [23]. On the other hand, the formation of nanocrystalline anatase under calcination was observed in the resulting TiO_2-PILC, similar to the result reported by Bagshaw et al. [15,16] whereas some other researchers did not observe the formation of anatase [11,17,18].

Conclusions.

The method of hydrolysis of $TiCl_4$ with HCl was applied to synthesize TiO_2-PILC. The structure of the resultant product is found to be primarily a mesoporous delaminated structure rather than a microporous pillared structure. The mesoporous delaminated structure results from the overlapping of titanium aggregates outside the clay interlayer region and clay particles. Both the textural analysis and the existence of the high *d* spacing in the low angle XRD pattern give proofs for the formation of the mesoporous delaminated structure. Based on these results, it could be concluded that the synthesis route by hydrolysis of $TiCl_4$ is possible to produce a disordered delaminated structure with both mesoporosity and microporosity.

On the other hand, the delaminated Ti pillared clay shows a good thermal stability under calcination condition. What also noteworthy is that calcination leads to the formation of nano-sized anatase which shows an unexpected high thermal stability beyond 1000 °C. Anatase nanoparticles formed in the delaminated Ti pillared Mts is of meaning for its catalytic applications, especially in the photocatalytic reaction in which anatase rather than rutile acts as the active component. In addition, the anatase nanoparticles might be attractive in improving the related reaction efficiency due to the nano-size effect.

Acknowledgments

Financial support from Natural Science Foundation of China (Grant No. 40372029), Natural Science Foundation (Grant No. 030471 and No. 04002140) of Guangdong Province, China, and from Foundation (Grant No. kfjj200503) of Key Laboratory for Nonferrous Materials and Processing Technology, Ministry of Education, China is gratefully acknowledged. The authors would like to thank Mr. F. Y. Wang, Mr. J. H. Yu, and Mr. X. N. Wen for their assistance in BET measurement and thermal analysis.

References

[1] G.W. Brindley, R.E. Sempels, Clay Miner. 12 (1977) 229.

[2] N. Lahav, U. Shani, J. Shabtai, Clays and Clay Miner. 26 (1978) 107.

[3] T.J. Pinnavaia, Science 220 (1983) 365.

[4] J.T. Kloprogge, J. Porous Mater. 5 (1998) 5.

[5] P. Cool, H. Y. Zhu, K. Cassiers, E. F. Vansant, Stud. Surf. Sci. Catal 154 (2004) 789.

[6] S. M. Auerbach, K. A. Carrado, P. K. Dutta, Handbook of Layered Materials, Marcel-Dekker: New York, 2004.

[7] Z. Ding, H.Y. Zhu, G.Q. Lu, P.F. Greenfield, J. Colloid Interf. Sci. 209 (1999) 193.

[8] C. Ooka, H. Yoshida, K. Suzuki, T. Hattori, Micropor. Mesopor. Mater. 67 (2004) 143.

[9] K. Shimizu, H. Murayama, A. Nagai, A. Shimada, T. Hatamachi, T. Kodama, Y. Kitayama,

Appl. Catal. B Env. 55 (2005) 141.

[10]S. Yoda, Y. Sakurai, A. Endo, T. Miyata, H. Yanagishita, K. Otake, T. Tsuchiya, J. Mater. Chem. 14 (2004) 2763.

[11]H. Yoneyama, S. Haga, S. Yamanaka, J. Phys. Chem. 93 (1989) 4833.

[12]H. G. Zhu, Z. W. Pan, B. Chen, B. Lee, S. M. Mahurin, S. H. Overbury, S. Dai, J. Phys. Chem. B 108 (2004) 20038.

[13]J. Ramirez, P. Rayo, A. Gutierrez-Alejandre, J. Ancheyta, M. S. Rana, Catal. Today 109 (2005) 54.

[14]V. Chhabra, V. Pillai, B.K. Mishra, A. Morrone and D.O. Shah, Langmuir 11 (1995) 3307.

[15]J. Sterte, Clays and Clay Miner. 34 (1986) 658.

[16]S.A. Bagshaw, R.P. Cooney, Chem. Mater. 5 (1993) 1101.

[17]P. Malla, S. Yamanaka and S. Komarneni, Solid State Ionics 32-33 (1989) 354.

[18]A. Bernier, L.F. Admaiai, P. Grange, Appl. Catal. 77 (1991) 269.

[19]A. Gil, A. Massinon, P. Grange, Micropor. Mater. 4 (1995) 369.

[20]E.M. Fanfan-Torres, E. Sham, P. Grange, Catal. Today 15 (1992) 515.

[21]H.L. Del Castillo, P. Grange, Appl. Catal. 103 (1993) 23.

[22]R.T. Yang, J.P. Chen, E.S. Kikkinides, L.S. Chen, Ind. Eng Chem. Res. 31 (1992) 1440.

[23]J.L. Valverde, A. de Lucas, P. Sanchez, F. Dorado, A. Romero, Appl. Catal. B-Environ. 43 (2003) 43.

[24]H.P. He, R.L. Frost, F. Deng, J.X. Zhu, X.Y. Wen, P. Yuan, Clays Clay Miner. 52 (2004) 350.

[25]M.J. Martinez-Ortiz, G. Fetter, J.M. Dominguez, J.A. Melo-Banda, R. Ramos-Gomez, Micropor. Mesopor. Mater. 58 (2003) 73.

[26]S.J. Gregg, K.S.W. Sing, Adsorption, Surface Area and Porosity, 2nd Ed., Academic Press, New York, 1982.

[27]J.H. De Boer, B.G. Linsen, T. Van der Plas, G.J. Zondervan, J. Catal. 4 (1965) 69.

[28]E.P. Barrett, L.G. Joyner, P.P. Halenda, J. Am. Chem. Soc. 73 (1951) 373.

[29]S. Lowell, J.E. Shields, M.A. Thomas, M. Thommes, Characterization of Porous Solids and Powders: Surface Area, Pore Size and Density, Kluwer Academic, Boston, 2004.

[30]R. Burch, C.I. Warburton, Appl. Catal. 33 (1987) 395.

[31]J.P. Chen, M.C. Hausladen, R.T. Yang, J. Catal. 151 (1995) 135.

[32]T.J. Pinnavaia, M.S. Tzou, S.D. Landau, R.H. Raythatha, J. Mol. Catal. 27 (1984) 195.

[33]C.F. Baes Jr, R.E. Mesmer, Hydrolysis of Cations, Wiley, New York, 1976.

[34]J.D. Ellis, G.A.K. Thompson, Inorg. Chem. 15 (1976) 3172.

[35]F. Bergaya, P. Gallot, R. Setton, H. Van Damme, in: Proceedings of 10th International Clay Conference, July 18-23, Adelaide, Australia, 1995, p151.

[36]F. Bergaya, J. Porous Mat. 2 (1995) 91.

[37]T. Mandalia, M. Crespin, D. Messad, F. Bergaya, Chem. Commun. 19 (1998) 2111.

[38]C. Clinard, T. Mandalia, D. Tchoubar, F. Bergaya, Clays Clay Miner. 51 (2003) 421.

[39]P. Levitz, D. Tchoubar, J. Phys. 2 (1992) 771.

[40]S.A. Bagshaw, E. Prouze, T.J. Pinnavaia, Science 269 (1995) 1242.

[41]E.F. Christabel, H. Yannick, V. Loic, Benedicte, Chem. Phys. Lett. 398 (2004) 414.

[42]M.L. Occelli, J.V. Senders, J. Lynch, J. Catal. 107 (1987) 557.

[43]S. Brunauer, L.S. Demming, W.S. Demming, E.J. Teller, J. Am. Chem. Soc. 62 (1940) 1723.

[44]P. Yuan, H. P. He, F. Bergaya, D. Q. Wu, Q. ZhouJ. X. Zhu, Micropor. Mesopor. Mate. 88 (2006) 8.

[45]K. Sing, D. Everett, R. Haul, L. Moscou, R. Pierotti, J. Rouquerol, T. Siemieniewska, Pure & Appl. Chem. 57 (1985) 603.

[46]N.A. Seaton. Chem. Eng. Sci. 46 (1991) 1895.

[47]A.M. Venezia, V. La Parola, A. Longo, A. Martorana, J. Solid State Chem. 161 (2001) 373.

[48]A.A. Gribb, J.F. Banfield, Amer. Miner. 82 (1997) 717.

[49]H. Zhang, J. F. Banfield, Amer. Miner. 84 (1999) 528.

[50]G.W. Brindley, J. Lemaitre, Thermal, Oxidation and Reduction Reactions of Clay Minerals, Longman Scientific & Technical, London, 1987.

Tables

Table 1
Main chemical composition (wt.%) of TiO_2-pillared clay samples

Sample	SiO_2	Al_2O_3	TiO_2	Fe_2O_3	CaO	MgO	Na_2O	K_2O	loss
Na^+-Mt	67.74	11.51	0.11	2.03	3.31	3.37	2.57	0.20	8.03
Ti-AD	43.45	9.04	25.57	0.50	0.29	2.32	0.13	0.05	18.66
Ti-EAD	44.12	8.29	23.84	0.56	0.26	3.09	0.04	0.07	19.73

Table 2
Textural properties of the starting Na^+-Mt and TiO_2-PILCs samples

Sample	S_{BET} (m^2/g)	$S_{ext.}$ (S_{micro}) (m^2/g) [a]	V_P (mL/g) [b]	$V_{\mu P}$ (V_{mP}) (mL/g) [c]	APD (nm) [d]
Na^+-Mt	35.1	—	0.14	—	15.8
Ti-AD-300	250.1	126.4 (123.7)	0.29	0.05 (0.24)	3.7
Ti-EAD-300	323.2	167.1 (156.2)	0.36	0.06 (0.30)	3.9

[a] $S_{ext.}$ = external surface area, evaluated from *t*-plot; surface area of micropore (S_{micro}) is obtained by subtracting $S_{ext.}$ from total surface area (S_{BET}).

[b] V_P = total porous volume.

[c] $V_{\mu P}$ = microporous volume, calculated by BJH method; Mesoporous volume (V_{mP}) = $V_P - V_{\mu P}$.

[d] APD = average pore diameter.

Figure Captions

Figure 1. Powder X-ray diffraction patterns of Na^+-Mt and TiO_2-pillared samples

Figure 2. Nitrogen adsorption isotherms (the insert) and pore diameter distribution curves of Ti-AD-300 and Ti-EAD-300

Figure 3. Schematic representation of the delaminated Ti pillared montmorillonites

Figure 4. Dependence of specific surface area and anatase grain size of TiO_2-pillared Mts on calcination temperature

Figure 5. TG, DTG, and DSC curves of Ti-AD and Ti-EAD

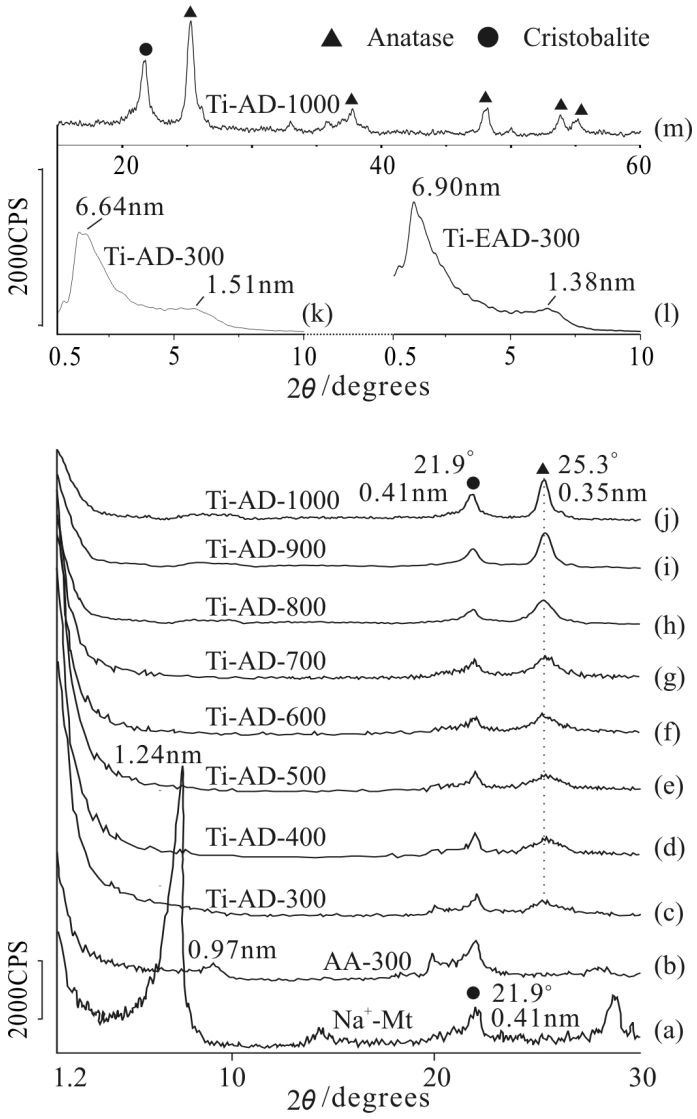

Fig. 1. Powder X-ray diffraction patterns of Na^+-Mt and TiO_2-pillared samples.

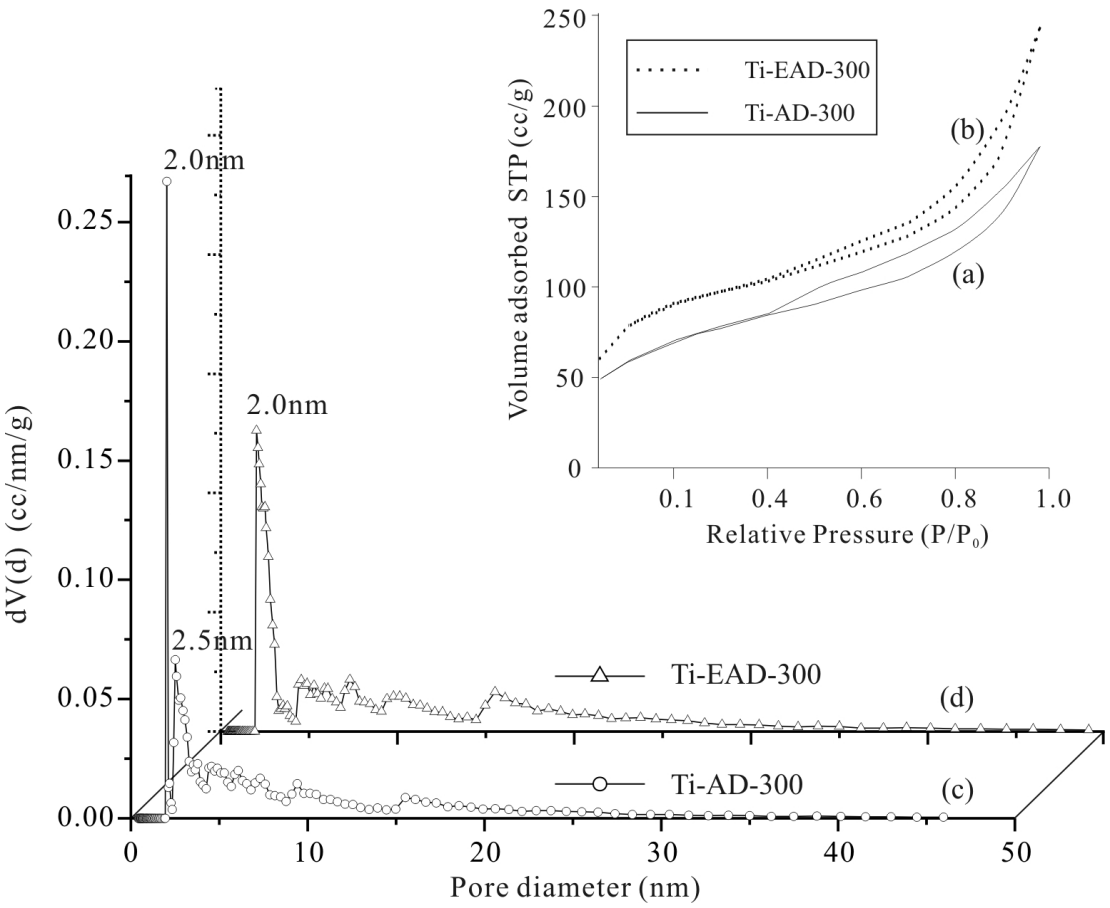

Fig. 2. Nitrogen adsorption isotherms (the insert) and pore diameter distribution curves of Ti-AD-300 and Ti-EAD-300

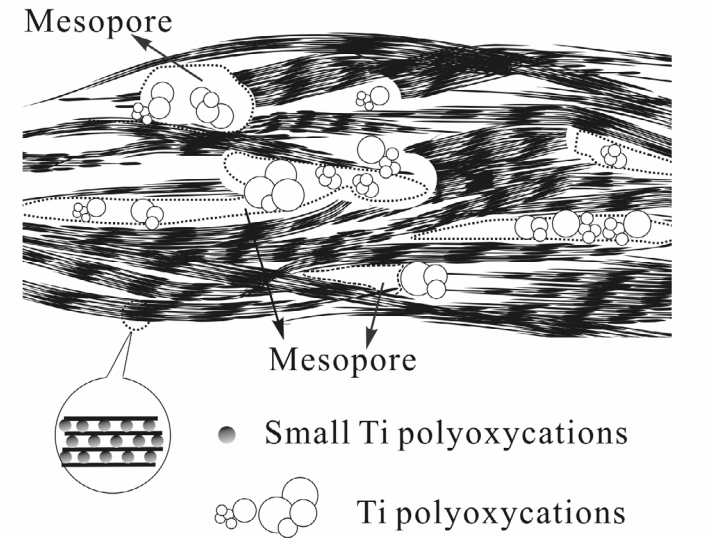

Fig. 3. Schematic representation of the delaminated Ti pillared montmorillonites

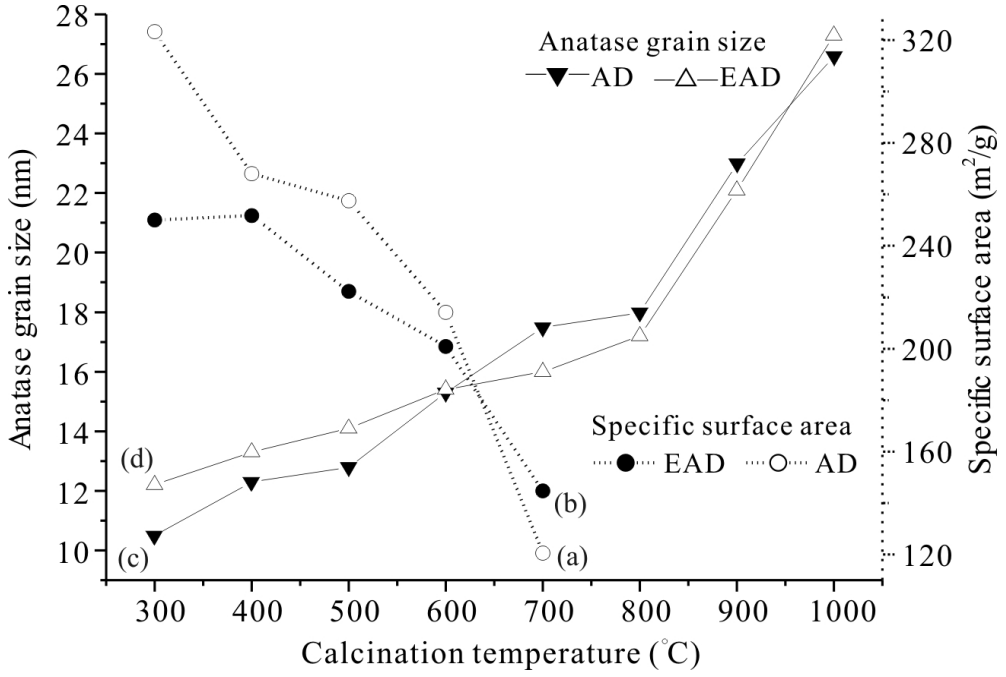

Fig. 4. Dependence of specific surface area and anatase grain size of TiO_2-pillared Mts on calcination temperature

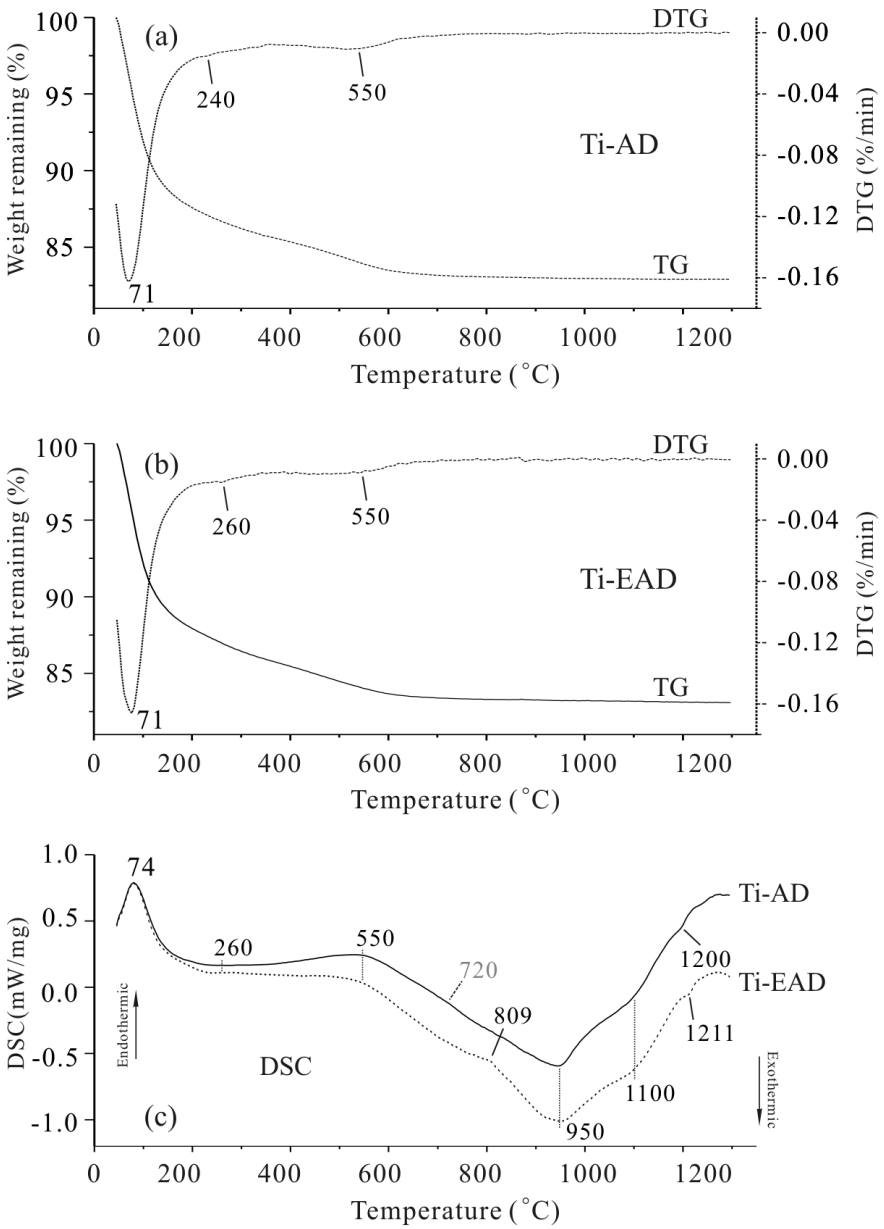

Fig. 5. TG, DTG, and DSC curves of Ti-AD and Ti-EAD